Supporting Information

Three-Dimensional Interconnected Core–Shell Networks with Ni(Fe)OOH and M-N-C Active Species Together as High-Efficiency Oxygen Catalysts for Rechargeable Zn-Air Batteries

Jiting Zhang, [a] Meng Zhang, [a] Lingxi Qiu, [a] Yan Zeng, [b] Jisheng Chen, [a] Ying Yu, [a] Chengzhou Zhu, [b] and Zhihong Zhu*[a]

[a] Institute of Nano-science and Nano-technology, College of Physical Science and Technology, Central China Normal University, Wuhan, 430079, China. E-mail: zhzhu@mail.ccnu.edu.cn

[b] Key Laboratory of Pesticide and Chemical Biology of Ministry of Education, International Joint Research Center for Intelligent Biosensing Technology and Health, College of Chemistry, Central China Normal University, Wuhan, 430079 P. R. China

I. Supplementary Texts

1. Materials preparation:

Synthesis of 3D Ni_xFe_y NPN: Prior to the start, 200 mL 0.1 M $NaBH_4$ solution was first bubbling N_2 for 30 min to remove oxygen from solution. Subsequently, 40 mL of metal precursor solution (0.1 M of total metal ions) with different Ni/Fe ratio was quickly injected into the above $NaBH_4$ solution with stirring in a water-sealed environment (Fig. 1a) for twenty minutes. Afterward, the resultant 3D Ni_xFe_y NPN (x/y is the molar ratio between Ni and Fe ions) were filtered and rinsed with deionized water. For comparison, we further synthesized 3D Ni and Fe NPN using $NiCl_2$•$6H_2O$ and $FeCl_3$•$6H_2O$ as metal precursors under the same process, respectively.

Synthesis of different ratio PANI coated Ni_2Fe_1 nanochain (Ni_2Fe_1@PANI-X): Add the

above 3D Ni_2Fe_1 NPN, 1.4 g aniline hydrochloride monomer and 10 ml alcohol together into 50ml 0.05M HCl solution, which was named as precursor solution A. The precursor solution A was then transferred to a round-bottomed flask in a thermostatic magnetic stirrer for 1 h at 0 °C. Meanwhile, the precursor solution B (2.5 g ammonium persulfate dissolved into 50ml 0.05M HCl) was placed in the 0 °C refrigerator for 1 hour. Finally, the precursor solution B was added to the above round-bottomed flask with magnetically stirred for 20h at a speed of 200 rpm. After filtering and freeze drying, Ni_2Fe_1@PANI-1 was obtained. Ni_2Fe_1@PANI-2, Ni_2Fe_1@PANI-3 were prepared through similar steps to Ni_2Fe_1@PANI-1 except using different weights of aniline hydrochloride monomer (0.75 g, 0.375 g, 0.1875 g) and ammonium persulfate (1.25g, 0.625 g, 0.3125 g) respectively.

Synthesis of interconnected core−shell Ni_2Fe_1@PANI-900-X and Ni_2Fe_1@PANI-KOH900: The Ni_2Fe_1@PANI-900-X (X = 1, 2, 3) hybrid was pyrolyzed at 900 °C for 2 h in Ar atmosphere at a heating rate of 5 °C/min. The synthetic route of Ni_2Fe_1@PANI-KOH900 was similar to Ni_2Fe_1@PANI-900-X, except that it was further immersed in 1 M KOH solution for 10 minutes before pyrolysis at 900 °C.

Synthesis of 3D interconnected Ni/Fe-N-C shell: To further study the ORR catalytic mechanism of carbon shell, 3D porous Ni/Fe-N-C shell was prepared by aqua regia etching of Ni_2Fe_1@PANI-KOH900 for 24.0 h to remove the Ni_2Fe_1 core. For comparison purpose, Ni_2Fe_1@PANI-900-Acid etching was also synthesized in a similar acid etching treatment of Ni_2Fe_1@PANI-900.

2. Physicochemical characterization: Field-emission scanning electron microscopy (FE-SEM, JSM-6700F, Japan) was employed to study the surface morphologies of samples. The N_2 adsorption-desorption isotherms and corresponding pore size distribution were measured on the V-Sorb 2800TP system. The crystal structure of the the products were identifed by XRD (X'Pert PRO MRD, PANalytical, the Netherlands). The TEM, STEM, HAADF-STEM

imaging and EELS atomic spectra were taken on a a Tecnai G2 F20 S-TWIN. Raman spectra were acquired using a confocal Raman microscope (LabRAM HR, JY-Evolution) with a laser of 532 nm. In situ raman spectra / electrochemical measurements was performed under controlled potentials using a homemade cell, which contained a working electrode (3 mm) sheathed at the bottom of the cell. The counter and reference electrodes were a Pt wire and a Ag/AgCl, respectively. A very thin and highly transparent polyvinyl chloride (PVC) film, which has almost consistent refractive index as water (n = 1.33), was used to protect working objective from the corrosive KOH electrolytes. XPS was analyzed on a Kratos AXIS Supra spectrometer.

3. Electrochemical measurements of ORR and OER: All electrochemical tests were performed by using a three-electrode on CHI760E electrochemical workstation (CH Instrument), and 95% iR-compensation was applied for the OER polarization curves. A platinum wire and Ag/AgCl (saturated KCl) electrode served as the counter electrode and reference electrode, respectively. All measured potentials (vs Ag/AgCl) were calibrated to the reversible hydrogen electrode (RHE) according to Nernst equation ($E_{RHE} = E_{Ag/AgCl} + 0.197 + 0.059 \times pH$).

To prepare the working electrode, 2 mg catalyst powder was dispersed in a mixture of 1 ml of water-isopropanol-Nafion solution (5wt %) solution with volume ratio of 8:2: 0.05, followed by ultrasonic treatment for at least 60 min to form catalyst ink. Afterward, catalyst ink (10 μL or 20 μL) was drop-casted onto the RDE (PINE, 5.0 mm in diameter) or RRDE (PINE, 5.61 mm in diameter) with a 0.10 mg cm^{-2} loading for ORR or a 0.20 mg cm^{-2} loading for OER, then followed by drying at room temperature. For comparison purpose, commercially RuO_2 and Pt/C (20 wt%) were employed as the control catalyst for OER and ORR, respectively.

Koutecky-Levich equation:

$$\frac{1}{J}=\frac{1}{J_L}+\frac{1}{J_k}=\frac{1}{B\omega^{1/2}}+\frac{1}{J_k} \qquad (1)$$

where J and J_K are the measured current density and kinetic current density, respectively. ω is the rotating speed of electrode in rad s^{-1}, the linearity between J^{-1} and $\omega^{-1/2}$ in O_2-saturated 0.1 M KOH can be derived from LSV curves at various rotation speeds and different potentials.

RRDE voltammetry was performed to determine the four-electron selectivity with a Pt ring potential at 1.50 V (vs RHE). The hydrogen peroxide yield ($\%H_2O_2$) and the electron transfer number (n) per oxygen molecule were calculated by the following equations:

$$\%(H_2O_2)=\frac{200\times I_r/N}{I_d+I_r/N} \qquad (2)$$

$$n=\frac{4\times I_d}{I_d+I_r/N} \qquad (3)$$

where I_d and I_r are the disk and ring currents, respectively, and N (= 0.37) is the ring collection efficiency of RRDE. EIS were conducted in 1M KOH at 1.55 V vs. RHE on a GCE with frequency from 100 kHz to 100 mHz and an amplitude of 5.0 mV.

4. Rechargeable Zn-air battery assembly: A homemade Zn-air battery configuration was displayed in Fig. S6, where catalysts loaded on nickel foam (thickness: 1 mm) as the air cathode with a loading of 0.5 cm^2. A polished Zn foil (purity>99.99%, thickness: 0.3 mm) was used as the anode. And a certain volume of 6 M KOH containing 0.2 M zinc acetate electrolyte served as the electrolyte. A Pt/C + RuO_2 mixture catalyst-based battery with the mass ratio of 1:1 was also fabricated for comparison purpose.

5. Flexible solid-state Zn-air battery assembly: The polyvinyl alcohol (PVA) electrolyte was prepared as follows: First, 1g PVA powder was dissolved in 20mL KOH solution (1.0 M) at 90 °C under stirring for 3 h. The above solution was then poured onto a plastic template to form a piece of transparent gel after thawing at room temperature. Then the flexible solid-

state Zn-air battery was assembled with as-prepared air cathode and Zn foil on the two sides of PVA gel, and a copper wire served as a current collector (Fig. 7g, inset).

II. Supplementary Fig.s and Tables

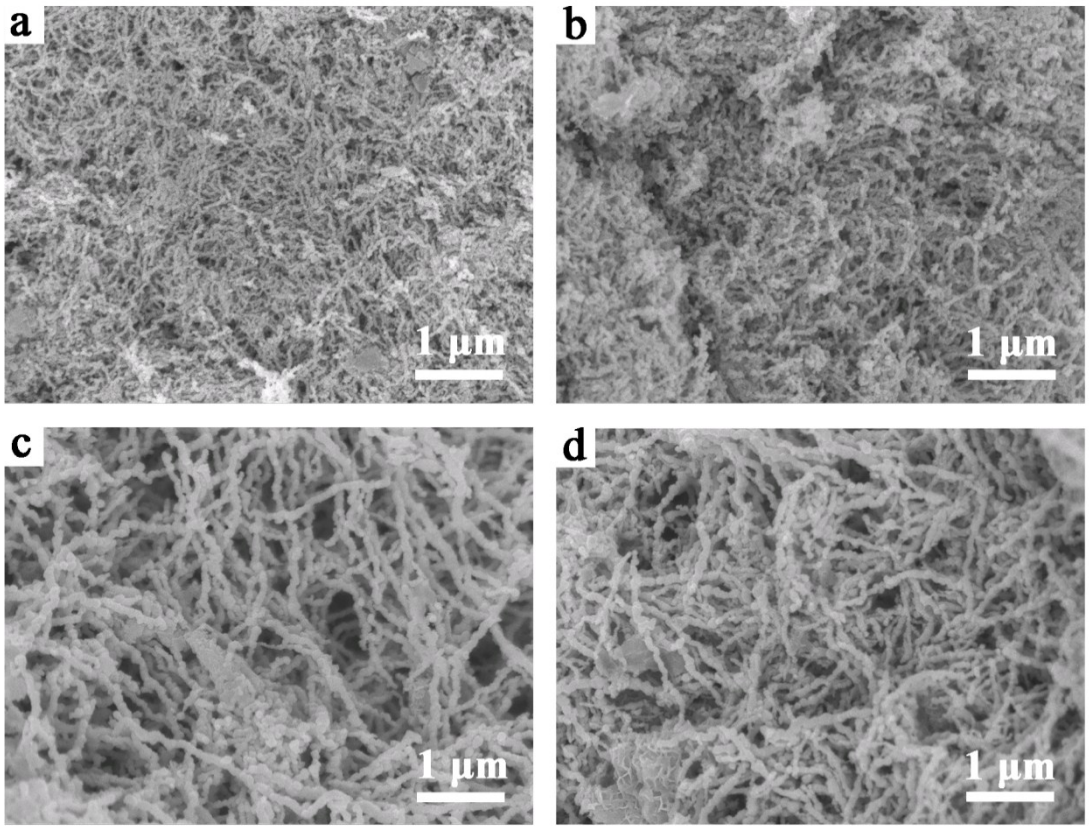

Fig. S1 SEM images of a) Ni NPN, b)Ni_1Fe_1 NPN, c)Ni_1Fe_2 NPN, and d) Fe NPN.

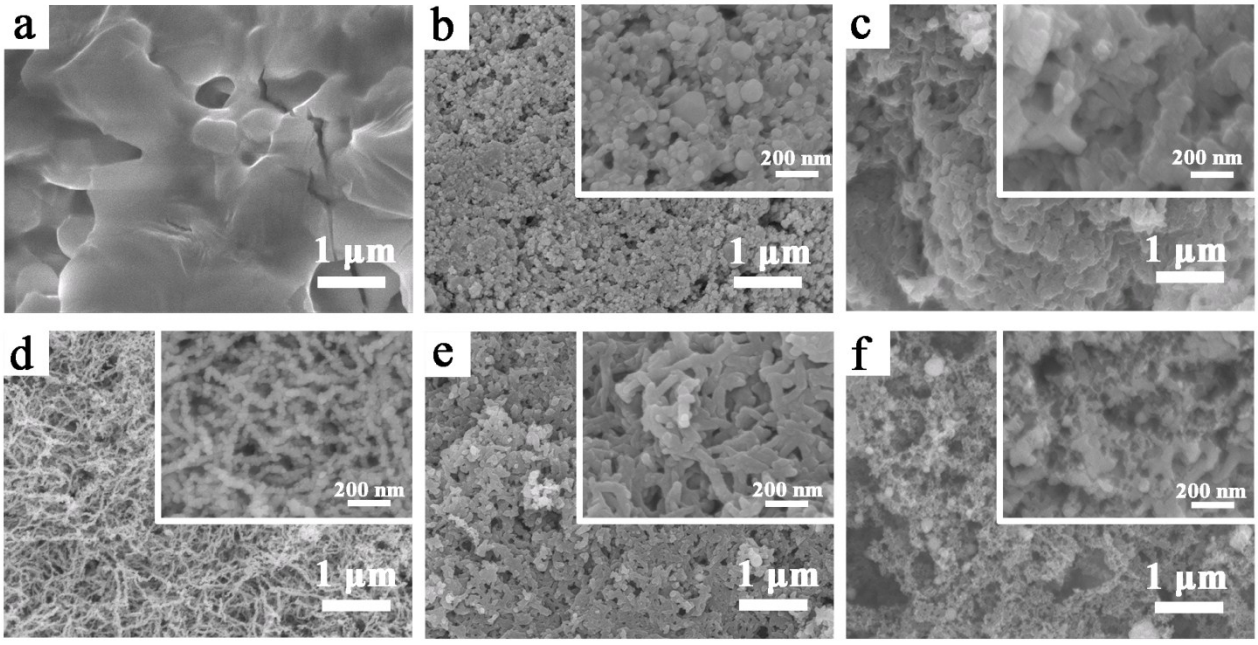

Fig. S2 SEM images of a) Ni_1Fe_1-900, b)Ni_1Fe_1@PANI-1, c)Ni_1Fe_2@PANI-3, d) Ni_2Fe_1 NPN, e) Ni_2Fe_1@PANI-900 and f) Ni_2Fe_1@PANI-KOH900.

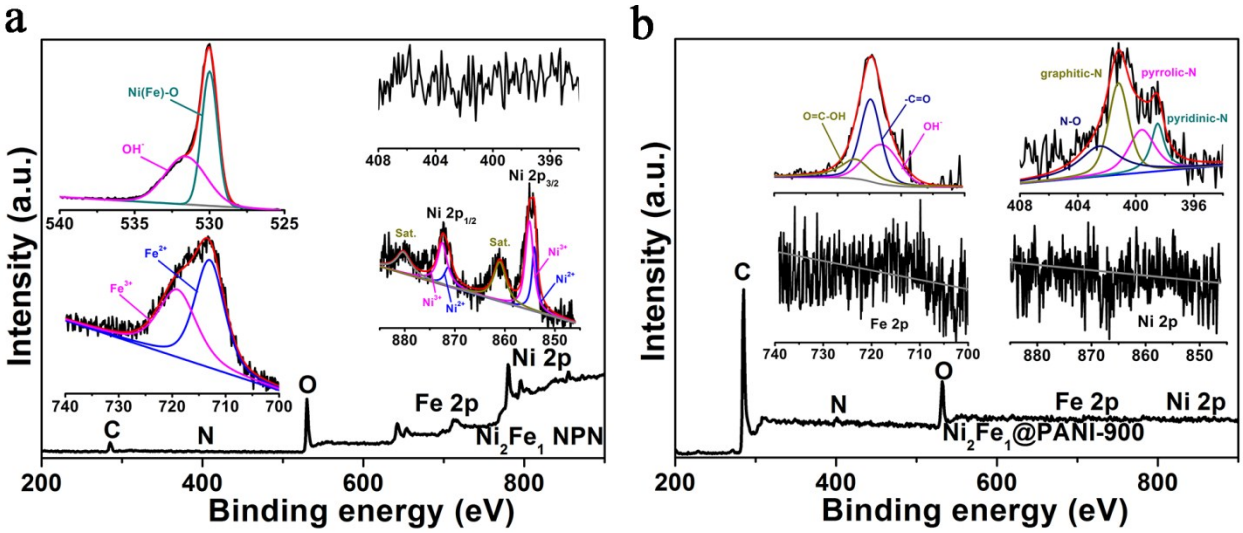

Fig. S3. XPS surface survey scan and the high-resolution O 1s, N 1s, Fe 2p, Ni 2p spectra of a) Ni_2Fe_1 NPN, b) Ni_2Fe_1@PANI-900.

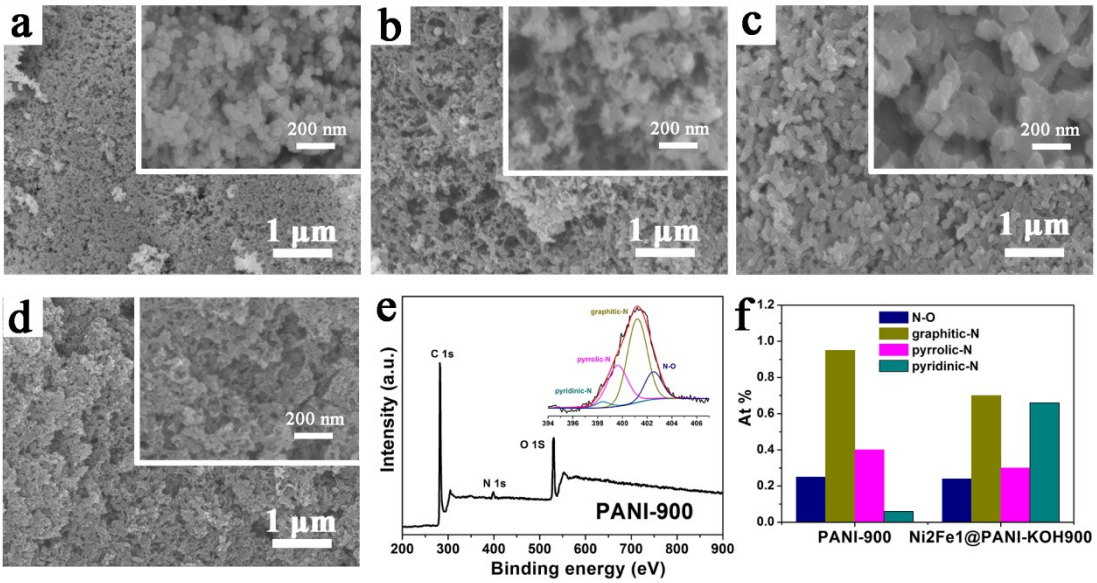

Fig. S4 SEM images of a) Ni_2Fe_1-after activation, b) Ni_2Fe_1@PANI-KOH900-after activation. c) Ni_2Fe_1@PANI-900-Acid etching and d) Ni/Fe-N-C shell. e) XPS surface survey scan and high-resolution N 1s of PANI-900. f) The relative at % of nitrogen atoms derived from XPS surface survey scan of PANI-900 and Ni_2Fe_1@PANI-KOH900.

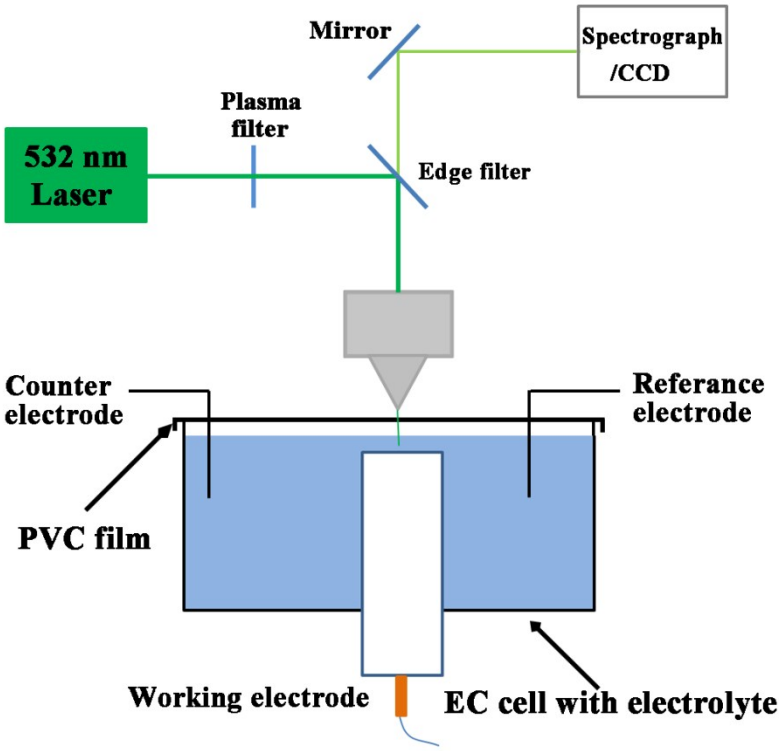

Fig. S5 Schematic diagram of the in situ electrochemical (EC) setup.

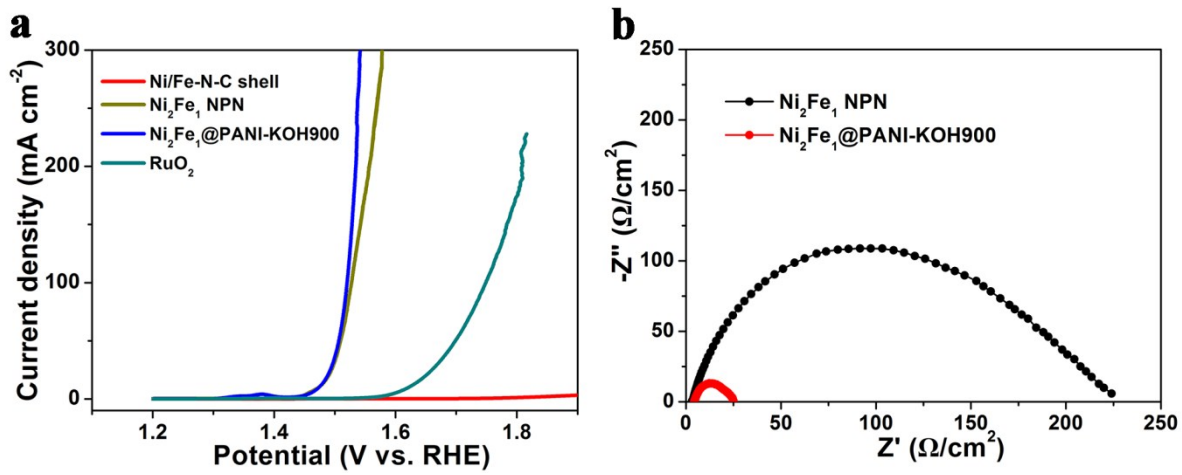

Fig. S6 a) LSV curves of Ni/Fe-N-C shell, Ni_2Fe_1 NPN, Ni_2Fe_1@PANI-KOH900 and RuO_2 toward OER. b) Nyquist plots of Ni_2Fe_1 NPNand Ni_2Fe_1@PANI-KOH900 in 1 M KOH at 1.55 V vs. RHE.

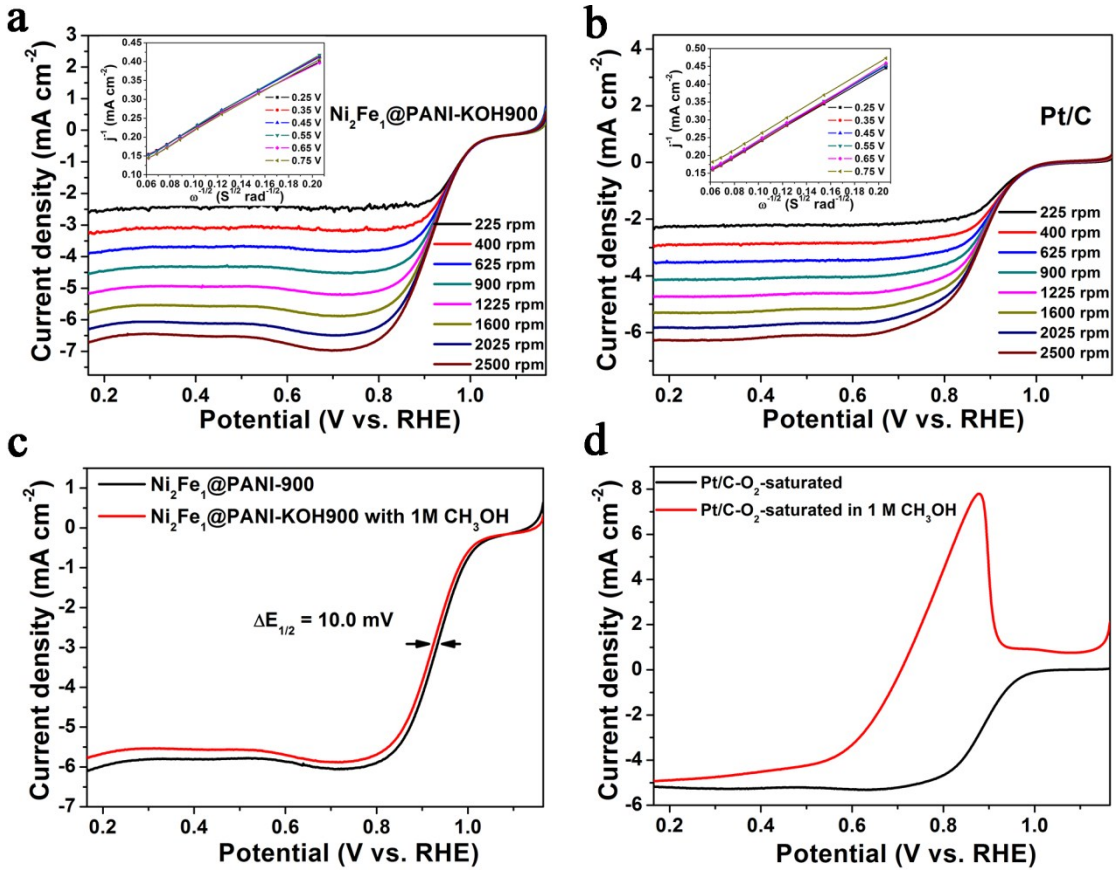

Fig. S7 LSV curves of a) Ni_2Fe_1@PANI-KOH900 and b) Pt/C in O_2-saturated 0.1 M KOH at various rotation speeds and the inset Fig. is K-L plots ($\omega^{-1/2}$ vs J^{-1}) at different potentials. LSV curves of c) Pt/C and d) Ni_2Fe_1@PANI-KOH900 in O_2-saturated 0.1 M KOH with and without 1 M methanol.

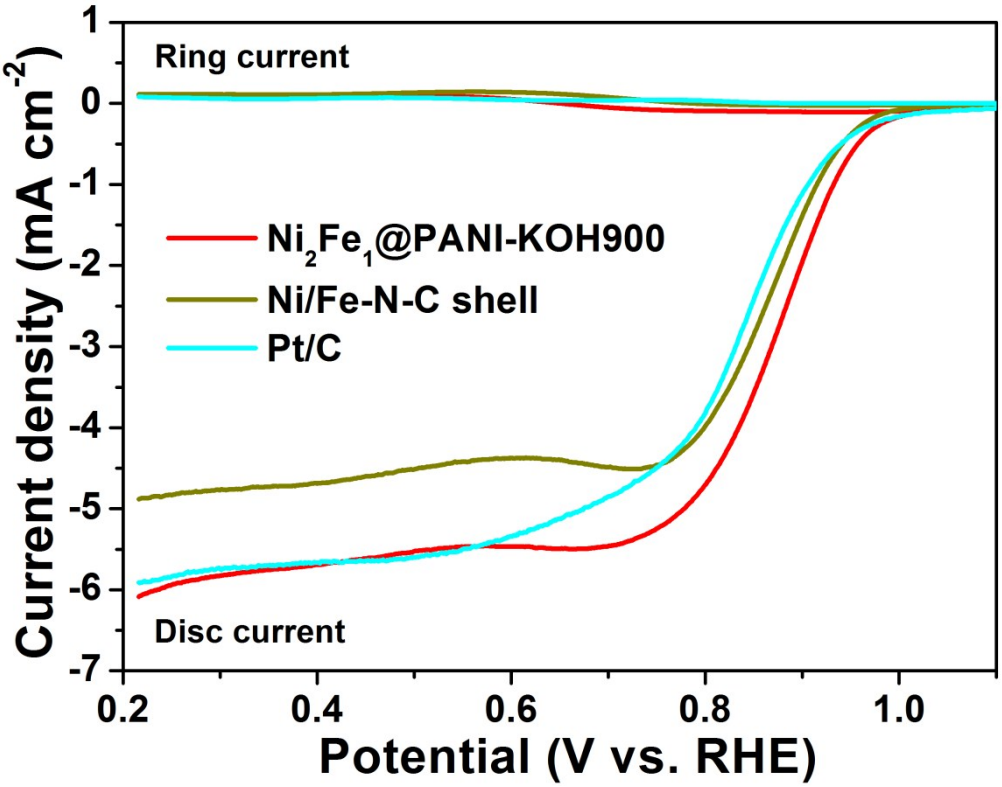

Fig. S8 RRDE measurements for Ni_2Fe_1@PANI-KOH900, Ni/Fe-N-C shell and Pt/C.

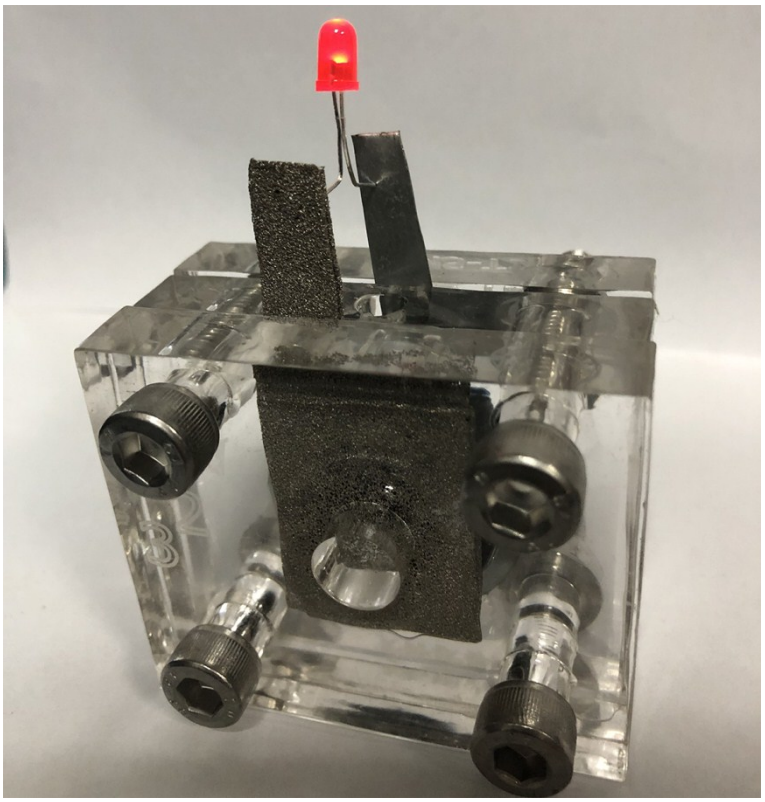

Fig. S9 Photo of a battery to power a red LED light in ambient air.

Table S1 Comparison of the bifunctional performance of Ni_2Fe_1@PANI-KOH900 with other electrocatalysts recently reported for ORR and OER.

Catalysts	$E_{1/2}$(V)	$E_{j=10}$(V)	ΔE(V) ($E_{i=10}$-$E_{1/2}$)	Ref.
PANI-900	**0.78**	**>1.8**	**>1.02**	**this work**
Ni_2Fe_1	**<0.4**	**1.64**	**>1.24**	**this work**
Ni_2Fe_1@PANI-KOH900	**0.92**	**1.47**	**0.55**	**this work**
Pt/C+RuO_2	**0.88**	**1.62**	**0.74**	**this work**
$Fe_{0.5}Ni_{0.5}$@N-GR	0.83	1.44	0.61	[1]
FeNi-NC	0.83	1.61	0.78	[2]
NiFe@NBCNT	0.83	1.425	0.68	[3]
Ni_3Fe-N Doped Carbon	0.79	1.63	0.84	[4]
NiFe@NC_x	0.86	1.55	0.69	[5]
NiFe-LDH/Co,N-CNF	0.790	1.542	0.752	[6]
Meso/micro-FeCo-N_x-CN-30	0.886	1.67	0.784	[7]
N-GCNT/FeCo-3	0.92	1.73	0.81	[8]
NiCo/PFC aerogels	0.76	1.62	0.86	[9]
NiO/CoN Porous NW	0.68	1.53	~0.85	[10]
NCNT/CoO-NiO-NiCo	0.83	1.5	0.67	[11]

$MnCo_2O_4$/NCNT	0.63	1.65	1.02	[12]
Ni-MnO/rGO aerogel	0.78	1.60	0.82	[13]

Table S2. Summary of rechargeable Zn-air batteries with non-noble-metal-based cathodes in 6.0 M KOH

Catalysts	charge/discharge voltage gap (V)	Cyclability	Ref.
$Pt/C+RuO_2$	**1.11@100**	**10 min /cycle for 200 cycles voltage increases ~0.66 V at the end**	**this work**
Ni_2Fe_1@PANI-KOH900	**0.90@100**	**10 min /cycle for 200 cycles voltage increases ~0.2 V at the end**	**this work**
NiFe@NBCNT	~0.80 V@10	600 s/cycle for 200 cycles negligible change of voltage at the end	[3]
NiFe@NCx	~0.80 V@10	600 s/cycle for 200 cycles voltage increases ~0.29 V at the end	[5]
Meso/micro FeCo-N_x-30	0.80@10	2h/cycle for 40h, negligible change	[7]
NCNT/CoO-NiO-NiCo	~0.86 V@20	600 s/cycle for 100 cycles negligible change of voltage at the end	[11]
CoO/N-CNT+NiFe LDH	~0.70@20	20 h/cycle for10 cycles, no significant voltage change	[14]

References

1. P. Liu, D. Gao, W. Xiao, L. Ma, K. Sun, P. Xi, D. Xue and J. Wang, *Adv. Funct. Mater.*, 2018, **28,** 1706928.
2. L. Yang, X. Zeng, D. Wang and D. Cao, *Energy Storage Mater.*, 2018, **12**, 277-283.
3. D. Bin, B. Yang, C. Li, Y. Liu, X. Zhang, Y. Wang and Y. Xia, *ACS Appl. Mater. Interfaces*, 2018, **10,** 26178-26187.
4. G. Fu, Z. Cui, Y. Chen, Y. Li, Y. Tang and J. B. Goodenough, *Adv. Energy Mater.*, 2017, **7,** 1601172.
5. J. Zhu, M. Xiao, Y. Zhang, Z. Jin, Z. Peng, C. Liu, S. Chen, J. Ge and W. Xing, *ACS Catal.*, 2016, **6**, 6335-6342.
6. Q. Wang, L. Shang, R. Shi, X. Zhang, Y. Zhao, G. I. N. Waterhouse, L.-Z. Wu, C.-H. Tung and T. Zhang, *Adv. Energy Mater.*, 2017, **7,** 1700467.
7. S. Li, C. Cheng, X. Zhao, J. Schmidt and A. Thomas, *Angew. Chem. Int. Ed.*, 2018, **57**, 1856-1862.
8. C.-Y. Su, H. Cheng, W. Li, Z.-Q. Liu, N. Li, Z. Hou, F.-Q. Bai, H.-X. Zhang and T.-Y. Ma, *Adv. Energy Mater.*, 2017, **7,** 1602420.
9. G. Fu, Y. Chen, Z. Cui, Y. Li, W. Zhou, S. Xing, Y. Tang and J. B. Goodenough, *Nano Lett.*, 2016, **16**, 6516-6522.
10. J. Yin, Y. Li, F. Lv, Q. Fan, Y.-Q. Zhao, Q. Zhang, W. Wang, F. Cheng, P. Xi and S. Guo, *ACS Nano*, 2017, **11**, 2275-2283.
11. X. Liu, M. Park, M. G. Kim, S. Gupta, G. Wu and J. Cho, *Angew. Chem. Int. Ed.*, 2015, **54**, 9654-9658.
12. A. Zhao, J. Masa, W. Xia, A. Maljusch, M.-G. Willinger, G. Clavel, K. Xie, R. Schloegl, W. Schuhmann and M. Muhlert, *J. Am. Chem. Soc.*, 2014, **136**, 7551-7554.

13. G. Fu, X. Yan, Y. Chen, L. Xu, D. Sun, J.-M. Lee and Y. Tang, *Adv. Mater.*, 2018, **30,** 1704609.
14. Y. Li, M. Gong, Y. Liang, J. Feng, J.-E. Kim, H. Wang, G. Hong, B. Zhang and H. Dai, *Nat. Commun.*, 2013, **4,** 2473.